

● *Original Contribution*

## ELASTIC PROPERTIES OF TENDON MEASURED BY TWO DIFFERENT APPROACHES

PO-LING KUO,\* PAI-CHI LI<sup>†</sup> and MENG-LIN LI<sup>†</sup>

\*Department of Physical Medicine and Rehabilitation, National Taiwan University Hospital, Taipei, Taiwan; and

<sup>†</sup>Department of Electrical Engineering, National Taiwan University, Taipei, Taiwan

(Received 3 January 2001; in final form 13 July 2001)

**Abstract**—Elastic properties of tendon were assessed by two different approaches. Six fresh bovine Achilles tendon specimens were used. The first approach directly measured Young's modulus along the transverse direction ( $E_{\text{perpendicular}}$ ) and the longitudinal direction ( $E_{\text{parallel}}$ ), using a cyclic compression–relaxation method. Young's moduli were derived based on the measured strain and stress values. The ratio of  $E_{\text{parallel}}:E_{\text{perpendicular}}$  at smaller strains was around 4 and decreased to 0.6–1.1 at larger strains. The second approach assumed that tendons are transversely isotropic. Three observable second-order elastic stiffness constants ( $c_{11}$ ,  $c_{13}$  and  $c_{33}$ ) were obtained by sound speed measurements along various propagation directions. The measured elastic stiffness constants were also correlated with results from the first approach. It was shown that the transverse isotropy assumption was valid at small strains. However, a significant discrepancy existed between the two approaches. The discrepancy was primarily due to viscoelasticity associated with the first approach. (E-mail: paichi@cc.ee.ntu.edu.tw) © 2001 World Federation for Ultrasound in Medicine & Biology.

**Key Words:** Tendon elasticity, Ultrasonic elasticity imaging, Transverse isotropy.

### INTRODUCTION

Tendon dysfunction is a major issue in rehabilitative medicine. The primary purpose of rehabilitation is to restore the mechanical functions of an injured or inflamed tendon. To noninvasively and quantitatively measure mechanical properties of tendon, sonoelastography has been proposed to monitor tendon functions during the rehabilitation process (Kuo et al. 1999).

Sonoelastography typically involves externally applied forces and reconstruction of strain fields. Several groups have published results in this research area (Cespedes et al. 1993; Emelianov et al. 1995; Gara et al. 1997; Kaisar and Ophir 1997; Kallel et al. 1996, 1997, 1998; Levinson et al. 1995; O'Donnell et al. 1994; Ponnekanti et al. 1994, 1995; Skovoroda et al. 1994, 1995; Sumi et al. 1995; Varghese and Ophir 1997a, 1997b, 1997c, 1998). One possible approach is based on a linear elasticity model under static deformation with small loadings. Elastic constants can then be reconstructed by a two-step inverse problem approach (Kallel and Bertrand 1996; Ophir et al. 1997; Skovoroda et al. 1994).

The first step involves estimating the strain fields from the ultrasound (US) data acquired pre- and postcompression. The second step is to find the optimal distribution of elastic modulus, given the estimated strain fields.

We have previously shown that axial components of the tendon's transverse strain fields could be measured by US with a baseband speckle-tracking algorithm. Compared to traditional B-mode imaging, strain imaging may be a better tool for clinical assessment of tendon disorders (Kuo et al. 1999). Given the strain fields, the next step is to reconstruct elastic properties of tendon. Because the strain fields are obtained by a compression method, knowledge of elastic modulus (*i.e.*, Young's modulus) distribution of tendon in compression is crucial. Unlike most biologic soft tissues, however, tendon possesses a strong axial symmetry with a unidirectional arrangement of collagen fibers reinforced throughout its entire thickness. Thus, the isotropic model used in most elasticity imaging for many other biologic tissues is not applicable. Instead, a transversely isotropic model used for materials exhibiting minimally hexagonal symmetry or maximally axial symmetry may be more feasible (Levinson 1987; Yoon and Katz 1976). Note that the transverse isotropy model can be reduced to the isotropy model if plane strain state can be created along the

Address correspondence to: Pai-Chi Li, Department of Electrical Engineering, National Taiwan University, No.1, Sec. 4, Roosevelt Road, Taipei, Taiwan. E-mail: paichi@cc.ee.ntu.edu.tw

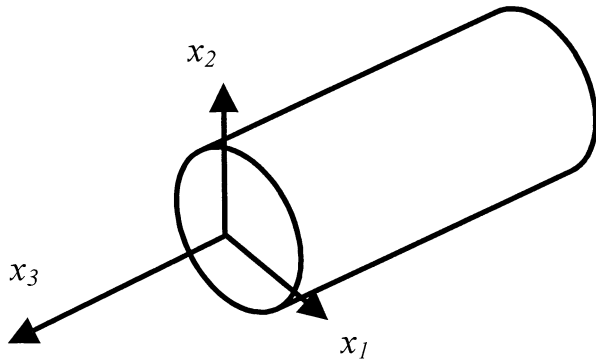


Fig. 1. Definition of coordinates.

longitudinal axis. In this case, reconstruction of elasticity properties can be greatly simplified. Thus, validation of the transverse isotropy assumption is of crucial importance in elasticity imaging of tendon.

For a transversely isotropic medium, mechanical properties such as Young's modulus depend on the angle between the stress axis and the fiber axis. In addition, values of Young's modulus along the longitudinal fiber axis (*i.e.*,  $E_{\text{parallel}}$ ) and along the direction perpendicular to the fiber axis (*i.e.*,  $E_{\text{perpendicular}}$ ) are both needed to describe the mechanical properties. Therefore, one main purpose of this study is to obtain the Young's modulus distribution of tendon and correlate it with the transverse isotropic model. Note that the Young's modulus is measured in compression in this paper so that it is in accordance with typical clinical applications of elasticity imaging. Also, linear elasticity is assumed. Under these conditions, the hypothesis that the tendon is transversely isotropic can be tested and the Young's modulus can be estimated based on observable elastic stiffness coefficients (Hoffmeister et al. 1996b; Levinson 1987). In this paper, data from both measurement approaches covering different strain states are correlated and potential sources of discrepancy are discussed.

## THEORY

A brief review of the constitutive equations used in the transversely isotropic model is described in the following (Hoffmeister et al. 1996b; Levinson 1987; Yoon and Katz 1976). Given the Cartesian coordinate ( $x_1, x_2, x_3$ ) with  $x_3$  representing the direction parallel to the fiber axis, a tendon is isotropic in the ( $x_1, x_2$ ) plane (Fig. 1). Thus, elastic properties of tendon can be described by an elastic stiffness tensor with hexagonal symmetry. The Young's modulus, defined as the ratio of the loading stress to the corresponding strain, can be derived from coefficients of the elastic stiffness tensor. Specifically,  $E_{\text{parallel}}$  (*i.e.*,  $E_{33}$ ) and  $E_{\text{perpendicular}}$  (*i.e.*,  $E_{11}$  and  $E_{22}$ ) can be written as:

$$E_{\text{parallel}} = c_{33} - \frac{c_{13}^2}{c_{11} - c_{66}} \quad (1)$$

and

$$E_{\text{perpendicular}} = 2c_{66} \left[ 2 - \frac{2c_{33}c_{66}}{c_{11}c_{33} - c_{13}^2} \right]. \quad (2)$$

Here,  $c_{ij}$  represents the elastic stiffness coefficients using the Voigt notation. Note that the sound velocity parallel (*i.e.*,  $V_{\text{parallel}}$ ) and perpendicular (*i.e.*,  $V_{\text{perpendicular}}$ ) to the fiber axis can be used to determine  $c_{33}$  and  $c_{11}$ . Furthermore, the elastic stiffness coefficient  $c_{13}$  can also be obtained from the phase velocity of longitudinal waves (*i.e.*,  $V_L$ ) propagating at any direction other than  $0^\circ$  and  $90^\circ$  in the plane containing the  $x_3$  axis. In other words,

$$c_{11} = \rho V_{\text{perpendicular}}^2, \quad (3)$$

$$c_{33} = \rho V_{\text{parallel}}^2, \quad (4)$$

and

$$c_{13} = \{ [(c_{33} \cos^2 \theta + c_{44} \sin^2 \theta)(c_{11} \sin^2 \theta + c_{44} \cos^2 \theta) - (c_{11} \sin^2 \theta + c_{33} \cos^2 \theta + c_{44})\rho V_L^2 + \rho^2 V_L^4]^{1/2} \} \times (|\sin \theta| |\cos \theta|)^{-1} - c_{44}, \quad (5)$$

where  $\rho$  is the tendon density and  $\theta$  denotes the angle relative to the  $x_3$  axis. Note that eqn (5) can also be rewritten as:

$$V_L = \{ (c_{11} \sin^2 \theta + c_{33} \cos^2 \theta + c_{44}) + [(c_{11} - c_{44})\sin^2 \theta - (c_{33} - c_{44})\cos^2 \theta]^2 + 4(c_{13} + c_{44})^2 \sin^2 \theta \cos^2 \theta \}^{1/2} (2\rho)^{-1/2}. \quad (6)$$

## MATERIALS AND METHODS

Samples used in this study were from fresh specimens of six bovine deep flexor tendons of the Achilles group. For each tendon, fat and residual tissue were carefully removed and the specimens were prepared for sound velocity measurements following the procedures described below. First, a cubic specimen was cut using a custom-made blade holder for measuring sound speeds parallel and perpendicular to the fiber axis. The blade holder was designed to keep two microtome blades parallel to each other with a separation of about 10.0 mm (measured by a dial caliper with a minimum scale of 0.02 mm). Typical specimens and the blade holder are illustrated in Fig. 2. The specimen was also used for direct measurements of Young's modulus along directions parallel and perpendicular to the fiber axis. Second, a rhom-

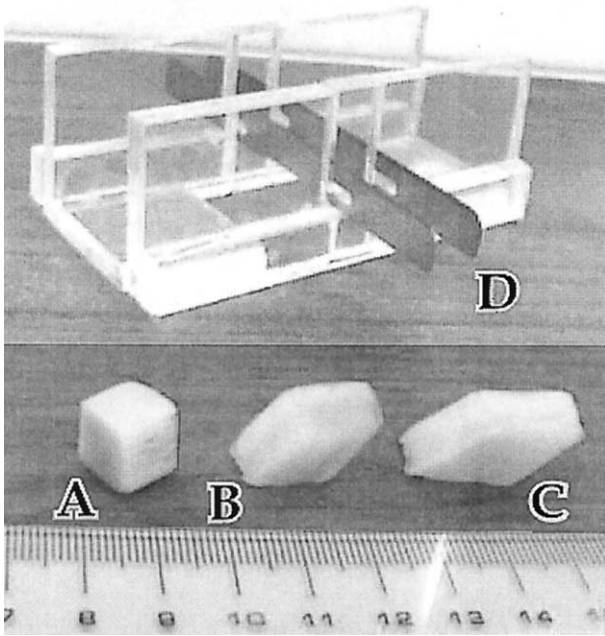


Fig. 2. Picture of the blade holder and typical specimens. Specimens with propagating directions (A) 0°, (B) 30°, and (C) 45° relative to the fiber axis; (D) the custom-made blade holder.

bohedron specimen was obtained using the blade holder at 30° relative to the longitudinal axis (*i.e.*, the propagation direction was perpendicular to the surface of the specimen and 30° relative to the longitudinal axis). Finally, another two rhombohedron specimens were prepared following similar procedures, except that the cutting angles were 45° and 60° relative to the longitudinal axis. Therefore, speeds of sound at five different propagating directions (0°, 30°, 45°, 60° and 90° relative to the longitudinal fiber axis) were measured for each tendon. For directions perpendicular to the fiber axis, velocities were measured at both  $x_1$  and  $x_2$  directions (see Fig. 1). Note that, in the transverse plane, the tendon shape is elliptic and the long axis was chosen as  $x_1$ . Size of the sample was confirmed using the dial caliper and then the sample was preserved in a normal saline solution for future use.

Two ultrasonic transducers were used for sound velocity measurements in the transmission mode. The center frequencies of the transmitter and receiver were 5 MHz (Panametrics V310, Waltham, MA) and 3.5 MHz (Panametrics V383), respectively. Note that sufficient overlap between the passband of the two transducers was present, such that accurate velocity estimates can be obtained. As shown in Fig. 3, the experiment setup had the receiving transducer attached to a custom-made acrylic holder. An acrylic enclosure was also used to hold water between the two transducers. An electronic balance with a readability of 0.1 g (OHAUS 1P12KS,

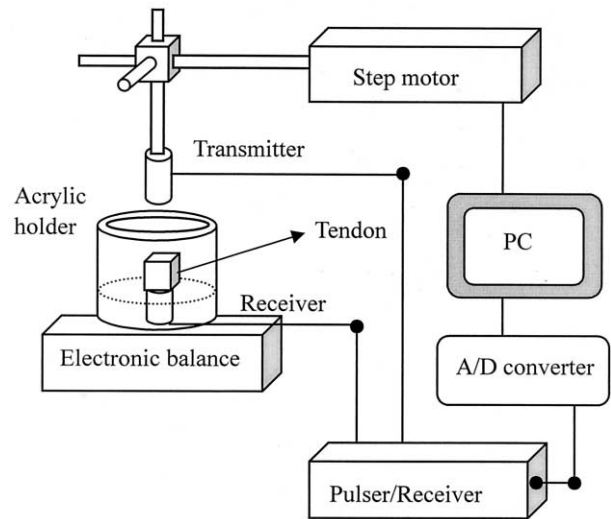


Fig. 3. Block diagram of the velocity measurement setup.

Florham Park, NJ) was placed under the acrylic holder to measure the applied load. The transmitting transducer was positioned by a computer-controlled, three-axis step motor system (Q-Sync, Hsin-Chu, Taiwan). Ultrasonic pulses were generated and received by a commercial pulser-receiver (Panametrics 5072PR). Settings of the pulser-receiver were chosen to optimize detection of the leading edge of the received ultrasonic waveform and avoid signal saturation.

A tendon sample was first placed on the center of the receiving transducer and the transmitting transducer was moved toward the upper surface of the specimen by the step motor system. To obtain speeds of sound at different strains, the ultrasonic signal was collected at three predetermined compression levels. First, the initial length (*i.e.*, the 0% strain state) was defined as the distance between the two transducers when the initial contact between the tendon and the transmitting transducer occurred. The initial contact was indicated when reading of the electronic balance started to increase. Second, the transmitting transducer was advanced by 475  $\mu\text{m}$ , which corresponded to a 4.7% strain. Note that stiffness of the measuring system (including the transducers, acrylic holder, and the electronic balance) is about 4-TPa, which is far larger than that of the tendon. Thus, deformation of the measuring system can be ignored when the tendon is compressed. Similarly, another advancement of the transmitting transducer by 475  $\mu\text{m}$  was defined as the 9.5% strain condition. The three ultrasonic signals were digitized at a sampling rate of 20 MHz by an A/D converter and stored in a personal computer for off-line analysis. After the measurements were completed, the sample was removed without changing the position of the transducers and water was filled

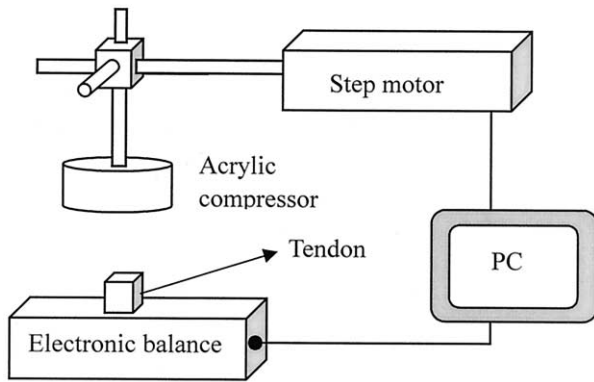


Fig. 4. Block diagram of the direct measurement setup.

into the acrylic holder between the two transducers. Another three ultrasonic measurements were made at the aforementioned three strain conditions by moving up the transmitting transducer and the acquired data were used to determine lengths of the sample given the speed of sound in water. For each sample, two repeated measurements were made at room temperature and data were acquired within 1 h.

The mass density of tendon samples, defined as weight divided by volume, was calculated using small samples removed from the tendons adjacent to the location where specimens had been cut. The electronic balance was used to determine the weight. Each sample was measured to the nearest 0.1 g. The volume of each sample was determined by a measuring glass with a minimum scale of 0.1 mL. For each sample, density was derived from the average of two repeated measurements.

For each tendon,  $E_{\text{parallel}}$  and  $E_{\text{perpendicular}}$  were obtained by using the setup shown in Fig. 4. Note that values of  $E_{\text{perpendicular}}$  along the  $x_1$  and  $x_2$  axes (*i.e.*,  $E_{11}$  and  $E_{22}$ ) were both measured. The setup consisted of the electronic balance, an acrylic plate positioned by the step motor system for compression and a personal computer for central control and data acquisition. Again, the stiffness of the whole measuring system (about 4-TPa) is far larger than that of tendon and the deformation of the measuring system was ignored without introducing additional errors in the measurements.

After putting each sample on the center of the electronic balance with its longitudinal fiber axis parallel or perpendicular to the surface of the balance, the acrylic compressor was carefully positioned toward the tendon sample. The compressor started to contact the sample when reading of the balance started to increase. The original height of each sample was determined beforehand using water measurements (*i.e.*, measurement obtained at 0% strain condition). The sample was then cyclically compressed at an average strain rate of

0.028/s. Each sample also received another cyclical compression along the fiber axis at an average strain rate at around 0.0004/s to determine influence of the strain rate on values of the Young's modulus. Note that the compressor was advanced stepwise and the actual compression speed was not constant. Nevertheless, the averaged strain rate can still be determined by the ratio of applied strain to the total time in each step. We had empirically found that the elastic stiffness of the tendon would decrease rapidly as the strain exceeded 12%. Hence, the maximum strain was limited to be under 11% for each sample. For the last sample, an additional compression procedure described as follows was used to determine the Young's modulus obtained by the incremental laws (Fung 1993). First, the sample was compressed sequentially to the three strain conditions (*i.e.*, 0, 4.7 and 9.5%). Second, at each strain condition, the sample was cyclically compressed at an average strain rate of 0.009/s with a maximum compression ratio of 2%. The small deformation produced an approximately linear stress-strain relationship.

Consecutive readings of the electronic balance were acquired at a rate of 2.5 Hz for every compression step and the readings were stored in a personal computer *via* a serial port. After completing six consecutive compression-relaxation cycles, each sample was kept in a normal saline bath for about 10 min. Data for various compression procedures and at various directions were acquired sequentially in a same manner. The area of tissue surface between the sample and the electronic balance was measured to calculate stress.

Given the sound velocity in water, the sound velocity in tendon along a specific direction can be derived from the equation:

$$V_{\text{tissue}} = V_{\text{water}} \times \frac{T_{\text{water}}}{T_{\text{tissue}}}, \quad (7)$$

where  $V_{\text{water}}$  represents the sound velocity in water at room temperature,  $T_{\text{tissue}}$  and  $T_{\text{water}}$  denote the times-of-flight with tissue and water in between the two transducers, respectively. For each recording, the time-of-flight was measured by detecting the time when the radiofrequency (RF) signal first exceeded a prespecified threshold. For all measurements, the threshold was 5 mV out of a 1-V signal dynamic range. This threshold was chosen so that accurate propagation time can be obtained without being affected by baseline noise.

Velocity measurements perpendicular (*i.e.*, along  $x_1$  axis) and parallel (*i.e.*, along  $x_3$  axis) to the longitudinal fiber axis of each sample were used to compute the elastic stiffness coefficients  $c_{11}$  and  $c_{33}$  according to eqns (3) and (4), respectively. The elastic stiffness coefficient

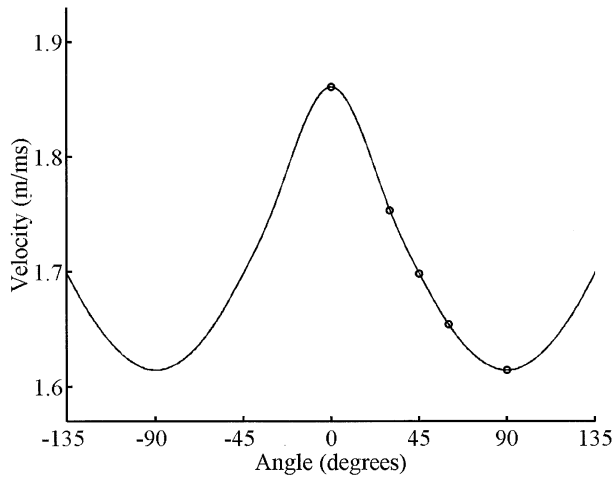


Fig. 5. Velocity interpolation. (○) Mean values of all samples at 0% strain.

$c_{13}$ , however, cannot be derived directly. The following procedures were taken to determine  $c_{13}$ . First, based on the assumption that tendon is transversely isotropic, values of sound velocity propagating at  $-135^\circ$ ,  $-45^\circ$  and  $135^\circ$  relative to the longitudinal fiber axis were assumed equal to those obtained at  $45^\circ$  relative to the longitudinal axis. Likewise, speeds of sound at angles of  $-120^\circ$ ,  $-60^\circ$  and  $120^\circ$  were equal to that at  $60^\circ$ , speed of sound at an angle of  $-30^\circ$  was equal to that at  $30^\circ$ , and speed of sound at  $-90^\circ$  was equal to that at  $90^\circ$ . Thus, as shown in Fig. 5, a velocity curve as a function of angle ranging from  $-135^\circ$  to  $135^\circ$  can be obtained using spline interpolation. Note that the convention used in the literature (Hoffmeister *et al.*, 1994) with the velocity along the  $x_1$  axis, being defined at  $90^\circ$  in the velocity curve, was adopted. Also note that the velocity curve is approximately monotonic from  $30^\circ$  to  $60^\circ$ . By using a  $1^\circ$  increment, there are totally 31 values that can be used to generate 31 corresponding  $c_{13}$  estimates based on eqn (5). The elastic stiffness coefficient  $c_{44}$ , which corresponds to the propagation of transverse mode ultrasonic waves through the tissue, was assumed to be negligible compared to  $c_{11}$ ,  $c_{33}$  and  $c_{13}$ . Thus,  $c_{44}$  was initially set to zero (Levinson 1987, Hoffmeister *et al.* 1995). The value of  $c_{44}$  was then varied over several orders of magnitude to check its effects on  $c_{13}$  estimation. Finally, each estimated  $c_{13}$  was applied to eqn (6), with the angle varying from  $30^\circ$  to  $60^\circ$ . Totally, 961 (*i.e.*, 31 times 31) velocity estimates were obtained. The  $c_{13}$  value with the minimal mean squared errors between the estimated velocity values and the interpolated curve was selected as the optimal  $c_{13}$  estimate.

$E_{\text{parallel}}$  and  $E_{\text{perpendicular}}$  in each tendon were computed from the slope of the stress-strain curve. The strain for each measurement was determined by the ratio of the

total deformation to the initial height. The corresponding stress was obtained by dividing the load by the area of contacting surface between the sample and the balance. Note that, although the time-dependent Young's modulus of a viscoelastic material such as tendon can be derived based on the relaxation function (Fung 1994), such an approach was not adopted in our study. Instead, we employed a simplified method similar to that reported by Chen and Novakofski (1996). This approach ignored the time-variation of stress at every step and the measurement results were adequate to determine the spatial relationship of elastic properties in tendon. In this approach, the total strain was first obtained at each step. Next, the maximum reading from the electronic balance for every compression step was used as the corresponding stress. Finally, an interpolated stress-strain curve was obtained by the spline method, and it was used to determine the tangent modulus (*i.e.*, Young's modulus) at the three predetermined strain conditions (*i.e.*, 0%, 4.7% and 9.5%). Note that the initial compression-relaxation cycle was used for preconditioning the tendon and the corresponding data were not included for estimation (Fung 1993). After preconditioning, the tangent moduli obtained in the last five cycles were very similar to each other and the mean value was chosen as the estimated Young's modulus.

The measured  $E_{\text{perpendicular}}$  (*i.e.*,  $E_{11}$ ) was used in eqn (2) along with  $c_{11}$ ,  $c_{33}$  and  $c_{13}$  to estimate  $c_{66}$  for each tendon. The estimated values of  $c_{66}$  were then used in eqn (1) to estimate  $E_{\text{parallel}}$  (*i.e.*,  $E_{33}$ ). The estimated and measured values of  $E_{\text{parallel}}$  were also used to calculate the error  $E_{33 \text{ error}}$ , defined as:

$$E_{33 \text{ error}} = \frac{mE_{33} - eE_{33}}{mE_{33}}, \quad (8)$$

where  $mE_{33}$  denotes the measured value and  $eE_{33}$  represents the estimated value of  $E_{33}$ . Note that two estimates of  $c_{66}$  can be obtained using eqn (2), but only the one corresponding to a smaller  $E_{33 \text{ error}}$  was chosen.

An important goal of this study was to derive Young's modulus at different strains. Because tendon is incompressible, compression applied along one axis introduces motion in the other directions. The actual displacement in different planes is hard to predict in an anisotropic material. To simplify computations, we employed sound velocities and Young's modulus measured at the same strains to obtain estimates of  $E_{33}$ . An example is illustrated as follows. First, speeds of sound at  $0^\circ$ ,  $30^\circ$ ,  $45^\circ$ ,  $60^\circ$  and  $90^\circ$  relative to the fiber axis measured at the 4.7% strain condition were employed to obtain estimates of elastic coefficients (*i.e.*,  $c_{11}$ ,  $c_{33}$  and  $c_{13}$ ). Next, these estimated coefficients were used together

Table 1. Summary of mass density and velocity measurements

Sample		A	B	C	D	E	F	Mean $\pm$ SD
$\rho$ (g/cm <sup>3</sup> )		1.12	1.16	1.12	1.12	1.12	1.10	1.12 $\pm$ 0.02
$V_0$ (m/s)	$S_0$	1823	1938	1899	1885	1830	1792	1861 $\pm$ 55
	$S_{4.7}$	1774	1835	1798	1809	1763	1734	1785 $\pm$ 36
	$S_{9.5}$	1723	1764	1721	1713	1696	1692	1718 $\pm$ 25
$V_{30}$ (m/s)	$S_0$	1732	1793	1761	1762	1765	1708	1753 $\pm$ 29
	$S_{4.7}$	1716	1739	1745	1725	1735	1706	1727 $\pm$ 14
	$S_{9.5}$	1651	1682	1682	1660	1674	1674	1670 $\pm$ 12
$V_{45}$ (m/s)	$S_0$	1676	1720	1725	1712	1694	1666	1698 $\pm$ 24
	$S_{4.7}$	1661	1692	1718	1676	1679	1662	1681 $\pm$ 21
	$S_{9.5}$	1620	1661	1678	1636	1633	1644	1645 $\pm$ 21
$V_{60}$ (m/s)	$S_0$	1638	1676	1702	1664	1633	1614	1654 $\pm$ 32
	$S_{4.7}$	1628	1667	1694	1648	1628	1609	1645 $\pm$ 31
	$S_{9.5}$	1617	1655	1670	1629	1597	1596	1627 $\pm$ 30
$V_{90(11)}$ (m/s)	$S_0$	1624	1630	1630	1615	1597	1584	1613 $\pm$ 19
	$S_{4.7}$	1620	1625	1625	1611	1591	1578	1608 $\pm$ 19
	$S_{9.5}$	1615	1621	1621	1605	1586	1553	1600 $\pm$ 26
$V_{90(22)}$ (m/s)	$S_0$	1615	1618	1608	1604	1585	1576	1601 $\pm$ 17
	$S_{4.7}$	1596	1612	1603	1600	1578	1570	1593 $\pm$ 16
	$S_{9.5}$	1592	1608	1597	1580	1573	1547	1583 $\pm$ 21

with the values of  $E_{11}$  at 4.7% strains derived from the stress-strain curve to obtain estimates of  $c_{66}$ . Finally, the estimated values of  $E_{33}$  at 4.7% strains were computed based on these estimates.

The influence of different strains on correlation of the two approaches was analyzed using a multivariate linear model (Littell et al. 1991). Let the column vector  $Y_i = [Y_{i1}, Y_{i2}, Y_{i3}]'$  represent the  $E_{33}$  error of the  $i$ -th sample for the three strain conditions. Assuming a multivariate normal distribution, the following model can be written:

$$Y_i = u + \varepsilon_i \quad (i = 1, 2, \dots, 6), \quad (9)$$

where the column vector  $u = [u_1, u_2, u_3]'$  is the mean response of all samples at the three strains and  $\varepsilon_i$  is the random error. Here,  $\varepsilon_i$  is assumed to be an independent and identical normal distribution with the mean equal to 0 and the covariance equal to 1; for example,  $\varepsilon_i \sim i.i.d. N_3(0,1)$  (Diggle 1988; Yonesh and Schork 1986).

Multivariate repeated-measures analysis of variance was applied to evaluate effects of strain variations. The null hypothesis for the independence of the strain conditions on  $E_{33}$  estimation is  $H_0: u_1 = u_2 = u_3$ . In other words, the null hypothesis assumes that the mean value of  $E_{33}$  error for all samples at zero strain (*i.e.*,  $u_1$ ) is equal to that at 4.7% (*i.e.*,  $u_2$ ) and that at 9.5% (*i.e.*,  $u_3$ ). Hence, we calculated the averaged sums of  $E_{33}$  error across all samples at each strain state (*i.e.*,  $u_1$ ,  $u_2$  and  $u_3$ ) and employed an  $F$ -test to test the null hypothesis. Furthermore, the probability of polynomial relations among strain effects was also analyzed. First, we transformed the values of  $E_{33}$  error into a  $2 \times 3$  matrix representing the linear and quadratic trends for  $E_{33}$  error at the three strain

levels (Littell et al. 1991). Next, univariate ANOVA tests were employed for each polynomial trend to determine its significance. A  $p$  value less than 0.05 was used to indicate statistical significance for all analyses.

## RESULTS

Results of mass density and velocity measurements for six tendons (*i.e.*, samples A, B, C, D, E and F) are summarized in Table 1, where  $\rho$  represents the mass density. The mean mass density of six tendons was 1.12 g, with an SD of  $\pm 0.02$  g. In Table 1,  $V_0$  denotes the sound velocity propagating along the fiber axis,  $V_{90}$  represents the velocity perpendicular to fiber axis, and

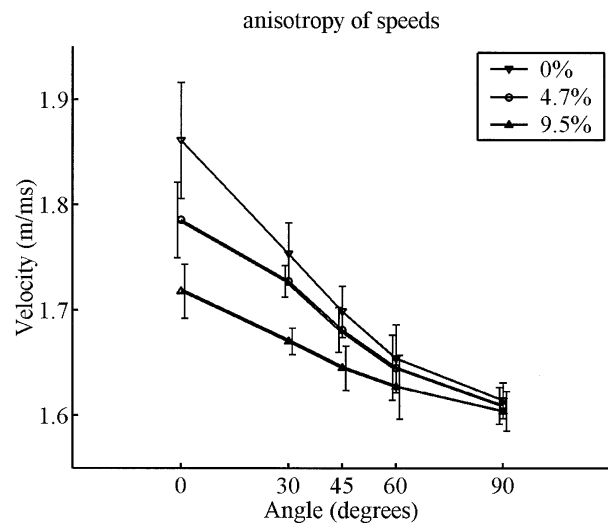


Fig. 6. Anisotropy of sound speeds. Error bars represent  $\pm 1$  SD.

Table 2. Summary of estimated elastic stiffness constants

Sample		A	B	C	D	E	F	Mean
$C_{11}$ (Gpa)	$S_0$	2.95	3.08	2.97	2.92	2.88	2.78	2.93
	$S_{4.7}$	2.94	3.06	2.95	2.90	2.86	2.76	2.91
	$S_{9.5}$	2.92	3.05	2.94	2.88	2.84	2.73	2.89
$C_{33}$ (Gpa)	$S_0$	3.72	4.35	4.04	3.98	3.78	3.53	3.90
	$S_{4.7}$	3.52	3.90	3.62	3.66	3.51	3.31	3.59
	$S_{9.5}$	3.32	3.61	3.31	3.28	3.25	3.15	3.32
$C_{13}$ (Gpa)	$S_0$	2.91	3.20	2.88	3.05	3.09	2.91	3.00
	$S_{4.7}$	2.94	3.22	3.23	2.99	3.13	2.96	3.08
	$S_{9.5}$	2.75	3.17	3.08	2.91	2.93	2.93	2.96

$V_{30}$ ,  $V_{45}$  and  $V_{60}$  denote the velocities at  $30^\circ$ ,  $45^\circ$  and  $60^\circ$  relative to the fiber axis, respectively. Note that  $V_{90(11)}$  and  $V_{90(22)}$  represent the sound velocities along the  $x_1$  and  $x_2$  axes, respectively.  $S_0$ ,  $S_{4.7}$  and  $S_{9.5}$  denote velocities obtained at the three strain conditions, 0%, 4.7% and 9.5%, respectively. Among the six tendons, results of velocity measurement agreed well with one another and velocities of all six tendons had the same gross dependency on angle. Generally speaking, the maximal speed occurred when the propagation was parallel to the longitudinal fiber axis (*i.e.*,  $0^\circ$ ). The velocity decreased as the angle relative to the fiber axis increased. It reached the minimum when it was perpendicular to the fiber axis. In Fig. 6, mean values of the measured speed were plotted as a function of angle, with the error bar representing  $\pm 1$  SD. Note that the degree of anisotropy (*i.e.*, the difference between  $V_0$  and  $V_{90}$ ) decreases as the strain increases. Also note that, in Table 1, the two speeds of sound measured perpendicular to the fiber axis (*i.e.*,  $V_{90(11)}$  and  $V_{90(22)}$ ) are similar to each other for each sample. In other words, the sound velocity measurement results are consistent with the transverse isotropy assumption.

Tables 2, 3 and 4 list results of estimated elastic stiffness coefficients, measured Young's moduli, estimated Young's moduli, estimated  $c_{66}$  and percentage of error between measured and estimated  $E_{33}$ . Definitions of  $S_0$ ,  $S_{4.7}$  and  $S_{9.5}$  are the same as those defined in Table 1. Again, angle dependence of elastic stiffness coefficients was clearly shown. In general, the mean value of

$c_{33}$  was the largest and  $c_{11}$  was the smallest, with  $c_{13}$  in between. The estimated  $c_{13}$  in each case also satisfied the relation  $c_{13}^2 < c_{11}c_{33}$ . In addition, we found that the estimated  $c_{13}$  changed monotonically as the angle varied from  $30^\circ$  to  $60^\circ$ . For all estimated  $c_{13}$  values, the average velocity error was less than 2 m/s between the estimated values, that is, estimates based on eqn (6), and the data from interpolation.

The measured Young's modulus also depended on angle. At 0% strain, all measured  $E_{\text{parallel}}$  values (*i.e.*,  $E_{33}$ ) were larger than the corresponding  $E_{\text{perpendicular}}$  values (*i.e.*,  $E_{11}$  and  $E_{22}$ ), with an average ratio of 4. Note that the values of  $E_{11}$  and  $E_{22}$  are similar at this strain condition. The ratios of  $E_{33}$  to  $E_{11}$  and  $E_{33}$  to  $E_{22}$ , however, seem to decrease at larger strains. At 4.7% strain, the ratios of  $E_{33}$  to  $E_{11}$  and  $E_{33}$  to  $E_{22}$  are 1.4 and 2.0, respectively. At 9.5% strain, the ratios of  $E_{33}$  to  $E_{11}$  and  $E_{33}$  to  $E_{22}$  become 0.6 and 1.1, respectively. In other words, the tendon becomes more transversely isotropic at small strains and becomes more isotropic at larger strains. The estimated values of  $c_{66}$  were about an order of magnitude lower than  $c_{11}$ ,  $c_{33}$ , and  $c_{13}$ . Compared with actual measurements, all the six values of Young's modulus estimated from  $c_{66}$  (*i.e.*,  $eE_{33}$ ) were significantly smaller. As shown in Table 4, however, there is a tendency that the percentage of estimated error of  $E_{33}$  (*i.e.*,  $E_{33 \text{ error}}$ ) decreases as the applied strain increases.

Statistical analysis results are summarized in Table 5. Row 1 lists effects of strain variations on  $E_{33 \text{ error}}$ .

Table 3. Summary of Young's modulus

Sample		A	B	C	D	E	F	Mean
$E_{11}$ (kPa)	$S_0$	30	17	29	56	54	22	35
	$S_{4.7}$	162	241	404	242	253	170	245
	$S_{9.5}$	610	1902	2149	1237	1324	1071	1382
$E_{22}$ (kPa)	$S_0$	30	17	30	49	55	22	34
	$S_{4.7}$	96	152	206	242	268	91	176
	$S_{9.5}$	394	884	1275	819	935	521	805
$E_{33}$ (kPa)	$S_0$	147	85	125	183	163	100	134
	$S_{4.7}$	194	179	348	435	412	366	322
	$S_{9.5}$	461	573	1078	828	792	1065	800

Table 4. Summary of estimated  $C_{66}$ ,  $E_{33}$  and percentage of estimation error in  $E_{33}$ 

Sample		A	B	C	D	E	F	Mean
$C_{66}$ (GPa)	$S_0$	0.71	0.73	0.92	0.57	0.35	0.38	0.61
	$S_{4.7}$	0.45	0.39	0.06	0.46	0.06	0.10	0.25
	$S_{9.5}$	0.73	0.26	0.08	0.30	0.20	0.007	0.26
$eE_{33}$ (kPa)	$S_0$	12	8	14	24	20	8	14
	$S_{4.7}$	58	88	126	91	80	53	83
	$S_{9.5}$	222	617	627	394	409	320	431
$E_{33}$ error (%)	$S_0$	91	90	88	87	87	91	89
	$S_{4.7}$	70	50	63	79	80	85	71
	$S_{9.5}$	49	7	41	52	48	69	44

Rows 2 and 3 represent the linear and quadratic trends between  $E_{33}$  error and strain, respectively. The results showed that the strain has a clear effect on  $E_{33}$  error, as indicated by the  $F$  value of 18.98 and  $p$  value of 0.0091. Moreover, the  $F$  value of 28.3 ( $p = 0.0031$ ) also implies that the linear effect of strain on  $E_{33}$  error is significant. On the contrary, the  $F$  value of 3.48 ( $p = 0.1212$ ) indicates that the quadratic component of strain effect is not as significant. In other words, strain variation has a significantly linear influence on the correlation of both approaches.

Table 6 shows influence of the strain rate on  $E_{33}$  measurements. In most strain conditions among the six samples, the  $E_{33}$  obtained at a slower strain rate was smaller than that determined at a higher strain rate. Table 7 lists the comparison of measured Young's moduli, estimated Young's moduli and percentage of the estimation error between values obtained by the simple compression procedure and incremental laws. All the measured Young's moduli obtained by incremental laws were larger than those obtained by the simple compression procedure. Also note that the percentage of the estimation error was smaller for results obtained by the incremental laws. The comparison of stress-strain curves along the  $x_3$  axis between the simple compression procedure and the procedure based on the incremental laws is shown in Fig. 7. A, B, C and D denote curves derived from initial strain state at 0%, 4.7%, 9.5% and 0% with a deformation range of 0% to 11%, respectively.

## DISCUSSION

In this paper, we successfully showed that tendon possesses transverse isotropy in the plane perpendicular

Table 5. Summary of statistical results

Effect	$F$ value	$p$ value
Strain	18.98	0.0091*
Linear trend	28.30	0.0031*
Quadratic trend	3.48	0.1212

\*  $p < 0.05$ .

to the fiber axis at small strains. Because it is relatively easy to create a plane strain state in tendon (Kuo et al. 1999), a transverse isotropy model greatly reduces the complexity in reconstruction of elastic parameters of tendon (Skovoroda et al. 1994). Although tendons are viscoelastic materials and the relaxation modulus or the storage modulus was not measured, the observations in this study are sufficient for future development of tendon elasticity imaging because linear elasticity can be applied to biologic tissues at small strains (Fung 1993). Moreover, we also showed that the degree of anisotropy decreases as the strain increases. Such a phenomenon may be due to the fact that fiber arrangement becomes irregular when tendon is compressed along the  $x_3$  axis. Because anisotropy of tendon primarily results from the axial arrangement of fibers along the  $x_3$  axis, irregularly arranged fibers consequently decrease the degree of anisotropy. Compression along the  $x_1$  or the  $x_2$  axis, on the other hand, does not significantly disturb the fiber arrangement.

The elastic stiffness tensor of formalin-fixed bovine Achilles tendons had been measured by Hoffmeister et al. (1994, 1995, 1996a). On the other hand, results of our study were based on fresh bovine Achilles tendons. The two studies have good agreement in mass density and anisotropy of velocity. Furthermore, the three elastic stiffness coefficients  $c_{11}$ ,  $c_{33}$  and  $c_{13}$  are at the same order of magnitude. However, dependence on angle,  $V_0$  and  $c_{33}$  was smaller in our study. Such a discrepancy may be explained by the fact that formalin fixation produces a measurable increase in longitudinal-mode ultrasonic velocity (Hoffmeister et al. 1994). Because the primary effect of formalin fixation on tissues is to bind together amino acids in the adjacent protein chain, this process may have a bigger impact along the fiber axis where protein chains are most reinforced. This results in a larger increase in velocity along the same direction.

An important feature of our study was to correlate the directly measured  $E_{33}$  values with those obtained from elastic stiffness coefficients. The discrepancies were large at small strains, but became smaller as the strain increased. Moreover, Hoffmeister et al. (1996b)

Table 6. Comparison of  $E_{33}$  measured at different strain rates

Sample		A	B	C	D	E	F	Mean
$E_{33}$ (kPa) Fast	$S_0$	147	85	125	183	163	100	134
	$S_{4.7}$	194	179	348	435	412	366	322
	$S_{9.5}$	461	573	1078	828	792	1065	800
$E_{33}$ (kPa) Slow	$S_0$	198	107	111	174	197	137	154
	$S_{4.7}$	212	160	158	247	177	100	175
	$S_{9.5}$	353	613	757	577	502	466	544

had derived Young's modulus from measurements of elastic stiffness tensor based on the linear elasticity model. The values of Young's modulus in their results were significantly larger than those directly measured in our study. Nevertheless, such results were reasonable, although the tendon consists of viscoelastic materials and the linear elasticity model inevitably introduces errors. Nonetheless, mechanical properties of the tendon obtained by the cyclical compression method can be approximated by assuming linear elasticity if the strain rate is fast enough (Hall *et al.* 1997). Generally speaking, the Young's modulus of a biologic tissue is larger if the viscous nature (*e.g.*, stress relaxation) plays a less significant role in a mechanical testing (Nordin and Frankel 1989). At a higher strain rate, the viscous loss becomes smaller and the measured Young's modulus can exceed that measured at a slower rate by several orders of magnitude (Abé *et al.* 1996). As reported by Hall *et al.* (1997), a strain rate faster than 0.5/s may be adequate to fairly describe the mechanical behavior of a biologic tissue as elastic. Therefore, it is reasonable to expect that the disagreement decreases as the strain rate increases. In this paper, strain rate dependence of Young's modulus was found. We also showed that increasing strain rate

significantly reduced disparity between the two approaches. In addition, the decrease at larger strains may also result from the fact that the viscous loss decreases as the measurement time increases.

Another important character of tendons is that the stress-strain relationship is nonlinear. Moreover, the tangent modulus at a specific strain state determined from the stress-strain relationship differs among curves obtained from different initial deformation conditions (Fung 1993). For example, the tangent modulus at 5% strain derived from the stress-strain curve obtained from a simple 0% to 11% strain cycle (*i.e.*, the initial strain-state is 0%) differs from that obtained by a small perturbation cycle around 5% strain (*i.e.*, the initial strain-state is 5%). One popular approach to determine the Young's modulus at a specific initial condition is to use the incremental laws. In other words, the sample is first deformed to the particular strain state, then a small cyclic perturbation is introduced to obtain the stress-strain relationship. In our study, we also studied the Young's modulus measurement based on the incremental laws and compared the results to the three initial strain con-

Table 7. Comparison of Young's modulus measurements between the simple compression procedure and the procedures based on incremental laws

		Simple procedure	Incremental procedure
$E_{33}$ (kPa)	$S_0$	99	220
	$S_{4.7}$	366	805
	$S_{9.5}$	1065	1452
$E_{11}$ (kPa)	$S_0$	22	103
	$S_{4.7}$	170	692
	$S_{9.5}$	1071	1807
$eE_{33}$ (kPa)	$S_0$	8	38
	$S_{4.7}$	53	215
	$S_{9.5}$	320	555
$c_{66}$ (GPa)	$S_0$	0.38	0.38
	$S_{4.7}$	0.10	0.10
	$S_{9.5}$	0.07	0.07
$E_{33}$ error (%)	$S_0$	91	82
	$S_{4.7}$	85	73
	$S_{9.5}$	70	61

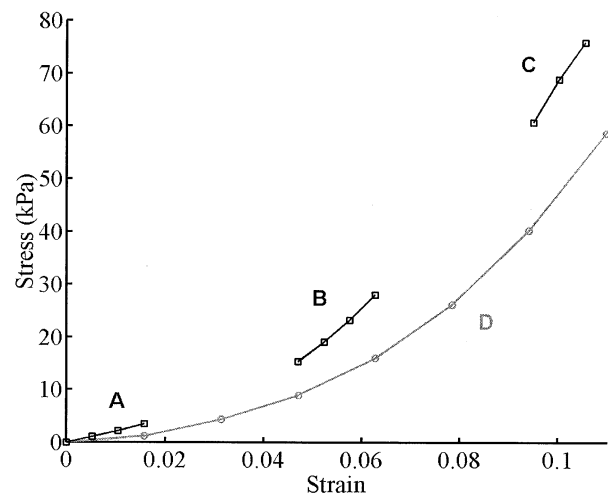


Fig. 7. Comparison of stress-strain curves between the incremental laws and the simple compression procedures. Curves derived by initial strain-state at (A) 0%, (B) 4.7%, (C) 9.5%, and (D) 0% with a range of 0% to 11% deformation.

ditions used in the velocity measurements. Results showed that the Young's modulus measurement based on the incremental laws had lower discrepancy between the two approaches. Such a conclusion, however, still needs to be verified by future experiments.

$c_{44}$  was neglected in our study. Because the reported shear stiffness values of most fresh biologic tissues are smaller than 5 MPa (Hoffmeister et al. 1996a), the  $c_{44}$  in our analysis was varied with a upper limit of 10 MPa, and we found that the change in  $c_{13}$  due to various  $c_{44}$  values was less than 1%. The result is also consistent with that reported in the literature (Hoffmeister et al. 1995).

In conclusion, we examined mechanical properties of fresh tendon specimens based on direct measurements and estimation from elastic stiffness constants. By direct measurements, we successfully showed that tendon exhibits transverse isotropy in the plane perpendicular to its fiber axis. In addition, estimation of elastic properties based on the transverse isotropy model may be applicable for tissues under a high strain rate. Such information is useful in further research work for tendon elasticity imaging.

*Acknowledgements*—Support supplied from the National Science Council of R.O.C. under Grant NSC 89 to 2213-E-002 to 041 is gratefully acknowledged. The authors also thank Dr. Ssu-Yuan Chen of National Taiwan University Hospital for his help in statistical analysis.

## REFERENCES

- Abé H, Hayashi K, Sato H. Data book on mechanical properties of living cells, tissues, and organs. New York: Springer-Verlag, 1996: 193–259.
- Céspedes I, Ophir J, Ponnekanti H, Maklad N. Elastography: Elasticity imaging using ultrasound with application to muscle and breast *in vivo*. *Ultrason Imag* 1993;15:73–88.
- Chen EJ, Novakofski J. Young's modulus measurements of soft tissues with application to elasticity imaging. *IEEE Trans Ultrason Ferroelec Freq Control* 1996;43:191–194.
- Diggle PJ. An approach to the analysis of repeated measurements. *Biometrics* 1988;44:959–971.
- Emelianov SY, Lubinski MA, Weitzel WF, et al. Elasticity imaging for early detection of renal pathology. *Ultrasound Med Biol* 1995; 21(7):871–883.
- Fung YC. *Biomechanics: Mechanical properties of living tissues*. New York: Springer-Verlag, 1993:259–263.
- Fung YC. *A first course in continuum mechanics*. New Jersey: Prentice-Hall, 1994:181–208.
- Garra BS, Céspedes I, Ophir J, et al. Elastography of breast lesion: Initial clinical results. *Radiology* 1997;202:79–86.
- Hall TJ, Bilgen M, Insana MF, et al. Phantom materials for elastography. *IEEE Trans Ultrason Ferroelec Freq Control* 1997;44:1355–1365.
- Hoffmeister BK, Gehr SE, Miller JG. Anisotropy of the transverse mode ultrasonic properties of fixed tendon and fixed myocardium. *J Acoust Soc Am* 1996a;99(6):3826–3836.
- Hoffmeister BK, Handley SM, Verdonk ED, Wickline SA, Miller JG. Estimation of the elastic stiffness coefficient  $c_{13}$  of fixed tendon and myocardium. *J Acoust Soc Am* 1995;97(5):3171–3176.
- Hoffmeister BK, Handley SM, Wickline SA, Miller JG. Ultrasonic determination of the anisotropy of Young's modulus of fixed tendon and fixed myocardium. *J Acoust Soc Am* 1996b;100(6):3933–3940.
- Hoffmeister BK, Verdonk ED, Wickline SA, Miller JG. Effect of collagen on the anisotropy of quasi-longitudinal mode ultrasonic velocity in fibrous soft tissues: A comparison of fixed tendon and fixed myocardium. *J Acoust Soc Am* 1994;96(4):1957–1964.
- Kaisar S, Ophir J. Reduction of signal decorrelation from mechanical compression of tissue by temporal stretching: Applications to elastography. *Ultrasound Med Biol* 1997;23(1):95–105.
- Kallel F, Bertrand M. Tissue elasticity reconstruction using linear perturbation method. *IEEE Trans Med Imag* 1996;15(3):209–213.
- Kallel F, Bertrand M, Ophir J. Fundamental limitations on the contrast-transfer efficiency in elastography: An analytic study. *Ultrasound Med Biol* 1996;22(4):463–470.
- Kallel F, Ophir J, Magee K, Krouskop T. Elastographic imaging of low-contrast modulus distributions in tissue. *Ultrasound Med Biol* 1998;24(3):409–425.
- Kallel F, Varghese T, Ophir J, Bilgen M. The nonstationary strain filter in elastography: Part II. lateral and elevational decorrelation. *Ultrason Med Biol* 1997;23(9):1357–1369.
- Kuo PL, Li PC, Shun CT, Lai JS. Strain measurements of rabbit Achilles tendons by ultrasound. *Ultrasound Med Biol* 1999;25(8): 1241–1250.
- Levinson SF. Ultrasound propagation in anisotropic soft tissue: The application of linear elasticity theory. *J Biomech* 1987;20(3):251–260.
- Levinson SF, Shinagawa M, Sato T. Sonoelastic determination of human skeletal muscle elasticity. *J Biomech* 1995;28(10):1145–1154.
- Littell RC, Freund RJ, Spector PC. SAS® system for linear models. 3rd ed. Cary, NC: SAS institute Inc., 1991:247–291.
- Nordin M, Frankel VH. *Basic biomechanics of the musculoskeletal system*. Philadelphia: Lea & Febiger, 1989:59–71.
- O'Donnell M, Skovoroda AR, Shapo BM, Emelianov ST. Internal displacement and strain imaging using ultrasonic speckle tracking. *IEEE Trans Ultrason Ferroelec Freq Control* 1994;41(3):314–25.
- Ophir J, Kallel F, Varghese T, et al. Elastography: A systems approach. *Int J Imaging Syst Technol* 1997;8:89–103.
- Ponnekanti H, Ophir J, Céspedes I. Ultrasonic imaging of the stress distribution in elastic media due to an external compressor. *Ultrasound Med Biol* 1994;20(1):27–33.
- Ponnekanti H, Ophir J, Huang Y, Céspedes I. Fundamental mechanical limitations on the visualization of elasticity contrast in elastography. *Ultrasound Med Biol* 1995;21(4):533–543.
- Skovoroda AR, Emelianov ST, Lubinski MA, et al. Theoretical analysis and verification of ultrasound displacement and strain imaging. *IEEE Trans Ultrason Ferroelec Freq Control* 1994;41(3):302–313.
- Skovoroda AR, Emelianov ST, O'Donnell M. Tissue elasticity reconstruction based on ultrasonic displacement and strain images. *IEEE Trans Ultrason Ferroelec Freq Control* 1995;42(4):747–765.
- Sumi C, Nakayama K, Suzuki A. Estimation of shear modulus distribution in soft tissue from strain distribution. *IEEE Trans Biomed Eng* 1995;42:193–202.
- Varghese T, Ophir J. Estimation tissue strain from signal decorrelation using correlation coefficient. *Ultrasound Med Biol* 1996;22(9): 1249–1254.
- Varghese T, Ophir J. A theoretical framework for performance characterization of elastography: The strain filter. *IEEE Trans Ultrason Ferroelec Freq Control* 1997a;44(1):164–172.
- Varghese T, Ophir J. Enhancement of echo-signal correlation in elastography using temporal stretching. *IEEE Trans Ultrason Ferroelec Freq Control* 1997b;44(1):173–180.
- Varghese T, Ophir J. The nonstationary strain filter in elastography: Part I. frequency dependent attenuation. *Ultrasound Med Biol* 1997c;23(9):1343–1356.
- Yeung F, Levinson SF, Parker KJ. Multilevel and motion model-based ultrasonic speckle tracking algorithms. *Ultrasound Med Biol* 1998; 24(3):427–441.
- Yonsh EF, Schork MA. Sample sizes in the multivariate analysis of repeated measurements. *Biometrics* 1986;42:601–610.
- Yoon HS, Katz JL. Ultrasonic wave propagation in human cortical bone—I. Theoretical considerations for hexagonal symmetry. *J Biomech* 1976;9:407–412.